Fermilab Library
0 1160 0033627 5
APR 18 199

DPNU-94-05
January 1994

Instability of an Accretion Flow with a Shock Wave

Koji Nobuta and Tomoyuki Hanawa
Department of Astrophysics, School of Science, Nagoya University, Chikusa-ku, Nagoya 464-01

(Received 1993 July 19 ; accepted 1994 January 4)

ABSTRACT

The dynamical instability of an accretion flow onto a black hole with a standing shock wave is investigated. When gas possessing angular momentum accretes onto a black hole, the flow can be associated with a standing shock wave. If the flow is decelerated at the pre-shock side of the front, the flow is unstable and the shock front leaves its equilibrium position. Assuming an isothermal accreting gas flow and the pseudo-Newtonian potential, we obtain the eigenvalues and eigenfunctions of unstable perturbations. The nonlinear evolution of the instability was also studied with a numerical simulation. The physical mechanism of the instability is explained in terms of shock wave propagation. It is shown that the motion of the shock front depends on the balance between the total pressures of the pre- and post-shock flows.

Key Words: Accretion — Black holes — Hydrodynamics — Instabilities — Shock waves

to appear in Publications of Astronomical Society of Japan (vol.46, No.3)

1. Introduction

Accretion of rotating gas onto a black hole is invoked for many active objects such as active galactic nuclei and black hole candidates in our Galaxy. It is widely accepted that gas spirals onto a black hole residing in the heart of these objects. Since the luminosities of these objects are highly variable over a wide range of time scales, the accretion onto a black hole is also likely to be variable and unstable. As a source of the variability we consider the instability of a steady rotating accreting flow onto a black hole in this paper.

Accretion flows in general suffer from several types of instabilities, such as dynamical, thermal, viscous and self-gravitating instabilities. These instabilities have been studied extensively by many authors. Besides these instabilities, an accretion flow with a shock wave may suffer from a new type of instability. Recently Nakayama (1992; 1993a) analyzed an accretion flow of a rotating gas onto a black hole and proved that a steady state flow with a standing shock wave is unstable when the pre-shock gas is decelerated at the shock front. This instability occurs in the inner region of the accretion disk. The growth time scale is roughly the sound crossing time scale in the accretion flow [$\tau \sim 3r_g/c_s \sim 3 \times 10^2\,(M/10^6\,M_\odot)\,(c_s/0.1\,c)^{-1}$ s]. Then we expect that this instability might be related to the x-ray luminosity variation on a short time scale since most of x-rays come from inner part of the accretion flow [See, e.g., the review by Oesterbrock (1991)].

The characteristics of this instability are not well known. The instability of the accretion flow with a shock wave was for the first time suggested by Fukue (1987) who found multiple solutions for a given set of model parameters such as accretion rate, gas temperature, and specific angular momentum [see also Abramowicz and Zurek (1981) for the suggestion of bimodal accretion of rotating gas onto a black hole]. At least one of the multiple solutions is likely to be unstable. Chakrabarti (1989b, c) and Nakayama (1992, 1993a) studied the linear stability of an accretion flow with a shock wave and obtained different results. The main difference comes from the boundary conditions imposed. Chakrabarti (1989b, c) considered a perturbation confined near the shock front, while Nakayama (1992; 1993a) assumed that the pre-shock (supersonic) flow is unchanged during the perturbation. Since no information goes upstream in a supersonic flow, Chakrabarti implicitly assumed an exponentially growing perturbation as the source of accretion while Nakayama considered an intrinsic instability of accretion flow with a shock wave. Although both types of instability may exist and contribute to time variability in AGN and X-ray binaries, we restrict ourselves to the intrinsic instability and adopt Nakayama's boundary conditions in this paper. This is because the intrinsic instability can be formulated consistently as an egienvalue problem. Nakayama (1992; 1993a) obtained the criterion for the instability and the upper and lower limits on the growth rate for an isothermal accretion flow. Eigenmodes of unstable perturbations, however, have not been obtained. In this paper we therefore study how the unstable perturbation grows in time.

Here we solve the perturbation equation as an eigenvalue problem. We obtain the eigenmodes of exponentially growing and damped perturbations. The computation methods are shown in section 2. Subsection 2.1 describes a model of accretion flow onto a black hole. Subsection 2.2 denotes the steady state solutions of the model. Subsection 2.3 is devoted to linear stability analysis around the steady state solutions. Linearized equations and boundary conditions are shown in subsection 2.3. Numerical procedures are shown in subsection 2.4 both for the linear stability analysis and for numerical simulation of nonlinear evolution. Numerical results of the linear stability analysis are described in section 3. The results of the numerical simulations are shown in section 4. We discuss the physical mechanism of this instability in terms of shock wave dynamics in section 5.

2. Model and Computation Methods

2.1. Accretion Flow onto a Black Hole

We considered a simple one-dimensional flow onto a black hole in order to study the instability of an accretion flow with a shock wave. We use non-relativistic fluid dynamics and the pseudo-Newtonian potential (Paczyński and Wiita 1981) for simplicity. The accretion flow is assumed to be axisymmetric in the cylindrical coordinates, (r, φ, z). Then the r-component of the equation of motion is expressed as

$$\frac{\partial v}{\partial t} + v\frac{\partial v}{\partial r} - \frac{\ell^2}{r^3} + \frac{1}{\rho}\frac{\partial P}{\partial r} + \frac{GM}{(r - r_g)^2} = 0\,, \quad (1)$$

along the equator. Here, v, ρ, P, ℓ, G, M, and r_g denote the r-component of the velocity, density, pressure, specific angular momentum, the gravitational constant, mass of the black hole, and the

Schwarzschild radius, respectively. The equation of mass conservation is expressed as

$$\frac{\partial \rho}{\partial t} + \frac{1}{r}\frac{\partial}{\partial r}(r\rho v) = 0\,, \tag{2}$$

under the assumption of a constant thickness (h) of the accretion flow in the z-direction. The assumption of constant thickness was employed for simplicity. See Chakrabarti (1989a) for the effects of variable thickness. In this paper we restrict ourselves to an isothermal inviscid flow with the sound speed, c_s, i.e., $P = \rho {c_s}^2$. See Matsumoto et al. (1984) and Chakrabarti (1990) for the effects of viscosity.

2.2. *Equilibrium Model*

When the flow is steady ($\partial/\partial t = 0$), it has a constant accretion rate, $\dot{M} \equiv -4\pi r h \rho v$, and a constant energy integral (except at the shock front),

$$E \equiv \frac{v^2}{2} + \frac{\ell^2}{2r^2} - \frac{GM}{r - r_g} - {c_s}^2 \ln\left(\frac{-rv}{r_g c_s}\right), \tag{3}$$

derived from the Bernoulli's theorem. The energy integral may be discontinuous only at a possible shock front. Only when E has a certain value, the flow can be transonic, i.e., can the flow velocity be subsonic in the outer region $r \gg r_g$ and supersonic in the inner region $|r - r_g| \ll r_g$.

It is pointed out by Fukue (1987) that equations (1) and (2) have multiple solutions for a given set of c_s and ℓ in some cases. Although he showed this using general relativity, the same is true for the post-Newtonian potential (see, e.g., Chakrabarti 1989b). Figure 1 shows an example of the multiple solutions for $c_s = 0.1\,c$ and $\ell = 1.87\,c r_g$, where c denotes the speed of light. The density and velocity are shown as a function of r for the outer shock wave, inner shock wave, and no shock wave solutions. In the pre-shock flow all the solutions have the same energy integral, $E = -0.0436\,c^2$. Also in the post-shock flow both the inner and outer shock wave solutions have the same energy integral, $E = -0.0573\,c^2$. They have the same density and velocity in the region of $r \geq 6.80\,r_g$. The inner and outer shock wave solutions have a standing shock wave at $r = 3.11\,r_g$ and $6.80\ r_g$, respectively while the density and velocity are continuous in the no shock wave solution. At the shock front, the so-called jump condition is fulfilled. All the solutions have a sonic point at $r = 44.46\,r_g$, which we call the outer sonic point in the following. The inner and outer shock wave solutions have another sonic point at $r = 2.36\,r_g$, which we call the inner sonic point.

Figure 2 shows the condition for the existence of the multiple solutions on the $c_s - \ell$ plane. There are triple solutions for a given set of c_s and ℓ in the dark region of figure 2. There is only one steady state solution, which has no shock wave, for c_s and ℓ in the blank region. On the right edge of the black region, the shock front and the sonic point coincide and the shock wave diminishes both in the inner and in the outer shock wave solutions. On the left edge the inner and outer shock wave solutions merge and disappear.

2.3. *Perturbation around the Steady Accretion*

In this subsection we consider a small perturbation around the steady state solutions with a standing shock wave. According to the standard method of linear stability analysis, we considered a normal mode where the density and velocity change according to the relations

$$\rho(r,\,t) = \rho_0(r) + \rho_1(r)\,e^{\sigma t}\,, \tag{4}$$

and

$$v(r,\,t) = v_0(r) + v_1(r)\,e^{\sigma t}\,, \tag{5}$$

respectively, where the growth rate (σ) and the eigenfunction (ρ_1 and v_1) are complex variables. Also the location of the shock front changes with time as $r = R + \xi\,e^{\sigma t}$.

The perturbation equations derived from equations (1) and (2) are expressed as

$$\sigma v_1 + \frac{\partial}{\partial r}(v_0 v_1) + {c_s}^2 \frac{\partial}{\partial r}\left(\frac{\rho_1}{\rho_0}\right) = 0\,, \tag{6}$$

and

$$\sigma\left(\frac{\rho_1}{\rho_0}\right) + v_0 \frac{\partial}{\partial r}\left(\frac{\rho_1}{\rho_0}\right) + v_0 \frac{\partial}{\partial r}\left(\frac{v_1}{v_0}\right) = 0\,. \tag{7}$$

In this paper we assumed that the perturbation has a finite amplitude only in the post-shock side of the flow. In other words, the pre-shock flow was assumed to remain unchanged during perturbation. This is because the pre-shock flow is supersonic between the outer sonic point and the shock front. No information comes from the down stream side when the flow is supersonic. Then the flow remains stationary unless the inflow (upstream) changes. In this paper we study a perturbation which grows intrinsically without change in the inflow. This assumption gives us a boundary condition at the shock front,

$$\mathcal{R} \equiv (2\sigma + \nu)\left(\frac{v_1}{c_s}\right) + \left[(\sigma + \nu)\left(\frac{{v_0}^{(post)}}{c_s}\right) + \sigma\,\frac{c_s}{{v_0}^{(post)}}\right]\left(\frac{\rho_1}{\rho_0}\right) = 0\,, \tag{8}$$

where

$$\nu \equiv -\frac{1}{v_0{}^{(post)}}\left[\frac{GM}{(R-r_g)^2} - \frac{\ell^2}{R^3} - \frac{{c_s}^2}{R}\right], \quad (9)$$

from the mass and momentum conservation at the shock front (Nakayama 1992).

The other boundary condition is set at the inner sonic point. Since equations (6) and (7) are singular at the inner sonic point ($r = r_s$), a regular solution must satisfy

$$\frac{\sigma}{c_s}\frac{\rho_1}{\rho_0} + \left[\frac{\sigma}{c_s} + 2\frac{d}{dr}\left(\frac{v_0}{c_s}\right)\right]\frac{v_1}{c_s} = 0\,, \quad (10)$$

there. We adopted equations (8) and (10) as boundary conditions and obtain σ as an eigenvalue.

The perturbation equations and boundary conditions are independent of the accretion rate. This is because both equations are proportional to density when the flow is isothermal. Thus, we do not specify the accretion rate in the following. The results shown in the following are valid for any accretion rate.

2.4. *Numerical Procedures*

In this paper we performed both the linear stability analysis and simulation of the nonlinear evolution of the instability using computer codes.

In the linear stability analysis, we solved equations (6) and (7) as a boundary value problem. For an assumed value of σ we integrated equations (6) and (7) from the inner sonic point to the shock front with the Runge-Kutta method. The initial value for the integration is given by the boundary condition (10). See appendix for the details of the initial condition and the Taylor expansion of the regular solution at the inner sonic point. By a tried and error method we searched for eigenvalues, σ, for which the numerical solution satisfies both equations (8) and (10).

In the simulation of the nonlinear evolution we integrated equations (1) and (2) with Van Leer's (1982) flux splitting method (see, e.g., the text book by Hirsch 1990). Equations (1) and (2) were integrated in the interval $2\,r_g \leq r \leq 50\,r_g$ with 1593 mesh points. The typical time step is taken to be $\Delta t = 0.06\,r_g/c$. The density and velocity are fixed at the outer boundary, $r = 50\,r_g$. Since the flow is supersonic at the inner boundary, the inner boundary condition does not need to be specified.

3. Linear Stability of Accretion Flow with a Shock Wave

We first study the stability of the inner shock wave solution for $c_s = 0.1\,c$ and $\ell = 1.87\,cr_g$. The left panel of figure 3 shows the left hand side of equation (8) as a function of σ. The ordinate and abscissa are the imaginary and real parts of σ in units of $-\nu = 0.185\,c/r_g$. The darkness denotes the sign of the real and imaginary arguments of the left hand side of equation (8), $\mathcal{R}_r$ and $\mathcal{R}_i$. Near the point $\mathcal{R} = 0$, both $\mathcal{R}_r$ and $\mathcal{R}_i$ change their sign and the eigenvalue σ appears as a quadruple point of four different colors in figure 3. We find 3 quadruple points at $\sigma = 0.031$ and $-0.152 \pm 0.088i\,c/r_g$ in the left panel of the figure 3. The positions of the eigenvalues are also shown as filled circles on the right panel of figure 3. Nakayama (1992) proved that the eigenvalue of an unstable mode is allowed to exist only in the grey regions in the right panel of figure 3. Figure 3 indicates that there is only one unstable mode for the inner shock wave solution. The numerically obtained growth rate of the unstable perturbation is consistent with the constraint, equation (27) of Nakayama (1993a).

Figure 4 shows the eigenfunction of the unstable mode ($\sigma = 3.10 \times 10^{-2}\,c/r_g$) for the inner shock wave solution of $c_s = 0.1\,c$ and $\ell = 1.87\,cr_g$. The ordinate and abscissa are the amplitude of the perturbation and the radial distance, respectively. The thick and thin curves denote ρ_1/ρ_0 and v_1/c_s, respectively. The growth rate and eigenfunction are real (not complex) for the unstable mode. When the perturbation has the amplitude shown in figure 4, the shock front is shifted inward ($\xi = -0.1\,r_g$). The change in the velocity is much smaller than the change in the density and the shift of the shock front.

Figure 5 is the same as figure 4 except for the damped oscillation [$\sigma = (-0.152 + 0.088\,i)\,c/r_g$]. The thick solid and dashed curves denote $\Re(\rho_1/\rho_0)$ and $\Im(\rho_1/\rho_0)$, respectively. In the damped oscillation the velocity perturbation is as large as the density perturbation, $v_1/c_s \sim \rho_1/\rho_0$. The density perturbation has a phase difference of $\sim \pi/2$ between the shock front and inner sonic point. The damped oscillation can be regarded as a sound wave trapped between the shock front and inner sonic point.

Figure 6 is the same as figure 3 but for the outer shock wave solution for $c_s = 0.1\,c$ and $\ell = 1.87\,cr_g$. Since $\nu > 0$ for the outer shock wave solution, all the eigenmodes are damped and the outer shock wave solution is stable (Nakayama 1992). The eigenvalues obtained are $\sigma = -0.0037$, $-0.0133 \pm 0.0469i$, and $-0.0227 \pm 0.1091i\,c/r_g$.

Figure 7 shows the growth rate of the unstable perturbation as a function of ℓ for a given c_s. The growth rate vanishes at the boundary of the existence of the triple solutions (see figure 2). This is consistent with the topological argument that one of the two adjacent solutions is unstable and the other is stable. When two adjacent solutions merge, they become neutrally stable.

4. Nonlinear Evolution of Unstable Perturbations

In this section we discussed the nonlinear evolution of perturbations around the steady state accretion solution on the basis of numerical simulations.

Figure 8 shows an example from our numerical simulations. Figures 8(a) and (b) show the time evolution of the density (ρ) and velocity (v), respectively. At the initial stage ($t = 0$) the eigenmode of the unstable perturbation is superimposed on the steady accretion flow of $c_s = 0.1\,c$ and $\ell = 1.87\,cr_g$. The shock front is shifted inward by $\xi = -6.0 \times 10^{-2}\,r_g$ from its equilibrium position, $R = 3.11\,r_g$ at the initial stage. According to the linear stability analysis, the perturbation grows exponentially in time $[\xi = -6.0 \times 10^{-2} \exp(0.031\,ct/r_g)\,r_g]$. The early stages of the nonlinear evolution qualitatively agree with the linear stability analysis.

The velocity of the post shock flow changes little while the density, mass flow, and shock front change appreciably. At $t = 55$ the shock front retreats to the inner sonic point ($r = 2.36\,r_g$). The velocity behind the shock wave exceeds the sound speed. Since no information goes upstream in the supersonic flow, the shock front forever goes down stream and the flow tends to the no shock wave solution. The mass flux is discontinuous at the shock front and higher in the post-shock side. The jump in the mass flux at the shock front increases with time. The excess in the post-shock mass flow is due to the shift of the shock front. The excess is supplied from the transition of the post-shock (dense) state to the pre-shock (less dense) state.

Figure 9 shows another example of a numerical simulation. The initial density distributions are similar to those of figure 8 except that the shock front is shifted outward by $\xi = 6.0 \times 10^{-2}\,r_g$. The early stages of the simulation are consistent with the linear stability analysis. In this model, the shock front approaches to $r = 6.80\,r_g$, i.e., the equilibrium position of the outer shock wave solution. Beyond $t \gtrsim 1000\,r_g/c$ the flow can be regarded as the outer shock wave solution.

In general, the flow approaches to either the no shock wave solution or the outer shock wave solution as long as the density and velocity are fixed in the outer region.

5. Discussion

In this section we discuss the physical mechanism for the instability of the accretion flow with a standing shock wave. Using the energy principle Nakayama (1993a) proved that this instability of an accretion flow with a shock wave is driven by the energy excess due to the change in the shock front. We thus consider the dynamics of the shock wave propagation.

Figure 10 shows the total pressure distribution in the steady state for $c_s = 0.1\,c$ and $\ell = 1.87\,cr_g$. The ordinate is the total pressure, $P_{tot} \equiv P + \rho v^2$. The abscissa is the radial coordinate. The thick and thin curves denote the pre- and post-shock flows, respectively. These curves intersect each other at $r = 3.11$ and $6.80\ r_g$, i.e., the equilibrium positions of a shock front. In the region $3.11\,r_g < r < 6.80\,r_g$ the total pressure is higher in the post-shock flow than in the pre-shock flow. Then the shock front is expected to move outward there. In the other regions $r < 3.11\,r_g$ and $r > 6.80\,r_g$ the total pressure is higher in the pre-shock flow and the shock front is expected to move inward. Accordingly, the shock front diverges from the unstable equilibrium position, $r = 3.11\,r_g$ and converges to the stable equilibrium position, $r = 6.80\,r_g$.

The above heuristic interpretation of the shock front dynamics is consistent with the rigorous stability criterion given by Nakayama (1992; 1993a). He proved that the steady flow is unstable when and only when ν is negative. The gradient of the total pressure is expressed as

$$\frac{\partial}{\partial r}(P + \rho v^2) = -\frac{1}{r}(P + \rho v^2) + \rho\left[-\frac{GM}{(r - r_g)^2} + \frac{\ell^2}{r^3} + \frac{{c_s}^2}{r}\right]. \qquad (11)$$

The difference in the total pressure gradient is evaluated as

$$\frac{\partial}{\partial r}\left[(P + \rho v^2)^{(pre)} - (P + \rho v^2)^{(post)}\right] = \nu\left[\rho^{(pre)} - \rho^{(post)}\right]{v_0}^{(post)} \qquad (12)$$

at the equilibrium position of the shock front, $r = R$. Equation (12) tells us that our heuristic interpreta-

tion totally agrees with the rigorous stability criterion. When $\nu < 0$, the pre-shock total pressure is higher inside $r < R$ (lower outside $r > R$) than the post-shock total pressure since $\rho^{(post)} > \rho^{(pre)}$ and ${v_0}^{(post)} < 0$. Thus the equilibrium position of $\nu < 0$ is unstable.

After the submission of the original manuscript, we found that Chakrabarti and Molteni (1993) had shown a similar argument. They related the instability to the change in the total pressure of the post-shock flow. As seen in equations (11) and (12), the total pressure gradient of the post-shock flow is dominant in the left hand side of equation (12) since $\rho^{(post)} > \rho^{(pre)}$. Thus their argument derives a similar but not the same stability criterion. As stated in their paper their argument cannot directly assert the stability of the inner shock wave solution for wind flow while our interpretation is coincident with the exact stability criterion.

Our heuristic interpretation of the shock wave dynamics may be extended for the case of an adiabatic shock wave with minor modification. Nakayama (1993b) has proved that his stability criterion is still valid for an adiabatic flow under some restrictions. When the flow is adiabatic, part of the kinetic energy is converted into the thermal energy and accordingly the total pressure of the post-shock flow at the shock front rises. When the shock front moves, the amount of energy conversion and accordingly the total pressure of the post-shock flow change. If the energy conversion is small, then Nakayama's criterion and our interpretation may still hold. In fact, the restrictions given in Nakayama (1993b) are on the entropy perturbation. He showed that the entropy change is not essential for most cases. Thus, we expect that our interpretation will be valid also for adiabatic shock waves.

We hope that our interpretation may help the understanding of accretion flow (and wind) with a shock wave in general. Although we assumed an stationary pre-shock flow in our stability analysis, pre-shock flow is also variable with time in reality. The next step for us is to include the change in the accretion rate and angular momentum in numerical simulation.

We thank Dr. Kunji Nakayama for stimulating discussions and showing us his analytical works before publication. We are grateful to an anonymous referee for calling our attention to Chakrabarti and Molteni (1993) and sending us the preprint before its publication. We also thank Dr. Lance T. Gardiner for reading the manuscript. This work is financially supported in part by the Grant-in-Aid for the Scientific Research (05640308) by the Japanese Ministry of Education, Culture, and Science.

Appendix Regular Solution at the Sonic Point

Equations (6) and (7) are singular at the sonic point where $v_0 = -c_s$. Then one of the two independent solutions is regular and the other is singular there. In this appendix we obtain the Taylor expansion of the regular solution up to the order of $\mathcal{O}[(r - r_s)^1]$. We need the values of v_1, ρ_1 and their gradient at the sonic point to start the numerical integration of equations (6) and (7) from the sonic point.

First we rewrite equations (6) and (7) as

$$\frac{dx}{dr} = \frac{1}{c_s + v_0}\left\{-\sigma x - \left(1 - \frac{c_s}{v_0}\right)\frac{dv_0}{dr}\cdot\left(\frac{x-y}{2}\right)\right\}, \tag{13}$$

$$\frac{dy}{dr} = \frac{\sigma}{2c_s}y, \tag{14}$$

where

$$x = \frac{\rho_1}{\rho_0} + \frac{v_1}{c_s}, \tag{15}$$

and

$$y = \frac{\rho_1}{\rho_0} - \frac{v_1}{c_s}. \tag{16}$$

Since the numerator of equation (13) should vanish at the inner sonic point, we have

$$\frac{dv_0}{dr}y = \left(\frac{dv_0}{dr} + \sigma\right)x \tag{17}$$

for the regular solution at the inner sonic point. By differentiating the numerator and denominator of equation (13) we obtain

$$\left(\sigma + 2\frac{dv_0}{dr}\right)\frac{dx}{dr} = -\frac{d}{dr}\left[\left(1 - \frac{c_s}{v_0}\right)\frac{dv_0}{dr}\right]\left(\frac{x-y}{2}\right) + \frac{dv_0}{dr}\frac{\sigma}{2c_s}y \tag{18}$$

at the inner sonic point. In our numerical computation we set $x = 1$ at the inner sonic point and computed y, dx/dr, dy/dr, and other variables and derivatives there using the above relations.

REFERENCES

Abramowicz, M. A., and Zurek, W. H. 1981, *Astrophys. J.*, **246**, 314.

Chakrabarti, S. K. 1989a, *Astrophys. J. Letters*, **337**, L89.

Chakrabarti, S. K. 1989b, *Mon. Not. Roy. Astron. Soc.*, **240**, 7.

Chakrabarti, S. K. 1989c, *Astrophys. J.*, **347**, 365.

Chakrabarti, S. K. 1990, *Mon. Not. Roy. Astron. Soc.*, **243**, 610.

Chakrabarti, S. K., and Molteni, D. 1993, *Astrophys. J.*, **417**, 671

Fukue, J. 1987, *Publ. Astron. Soc. Japan*, **39**, 309.

Hirsch, C. 1990, *Numerical Computation of Internal and External Flows vol. 2*, (John Wiley, Chichester), p. 420.

Matsumoto, R., Kato, S., Fukue, J., and Okazaki, A. T. 1984, *Publ. Astron. Soc. Japan*, **36**, 71.

Nakayama, K. 1992, *Mon. Not. Roy. Astron. Soc.*, **259**, 259.

Nakayama, K. 1993a, *Publ. Astron. Soc. Japan*, **45**, 167.

Nakayama, K. 1993b, private communication

Osterbrock, D. E. 1991, *Rep. Prog. Phys.*, **54**, 579.

Paczyński, B. and Wiita, P. J. 1980, *Astr. Astrophys.*, **88**, 23.

Van Leer, B. 1982, in *Proc. 8th International Conference on Numerical Methods in Fluid Dynamics*, (Springer, Berlin)

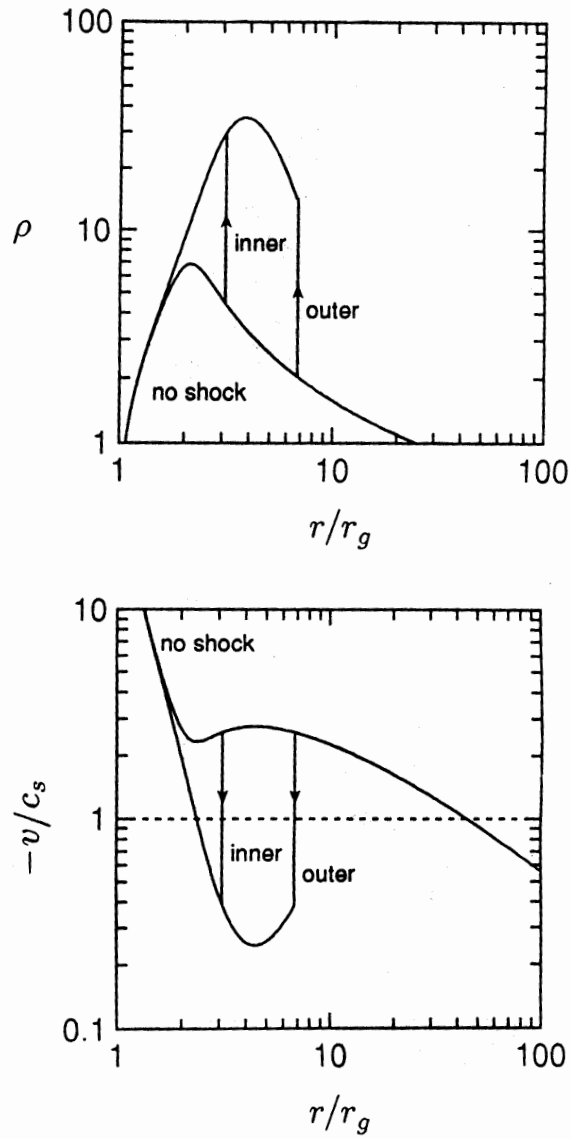

Fig. 1.— Steady state solutions for accretion flow onto a black hole. The upper and lower panels show the density (ρ) and velocity (v/c_s) distribution, respectively, as a function of the radial distance, r. The sound speed and specific angular momentum are taken to be $c_s = 0.1\,c$ and $l = 1.87\,r_g c$, respectively. The shock front is located at $r = 3.11\,r_g$ and 6.80 r_g in the inner and outer shock wave solutions, respectively. All the three solutions pass through the outer sonic point at $r = 44.46\,r_g$ while only the inner and outer shock wave solutions pass through the inner sonic point at $r = 2.36\,r_g$.

This 2-column preprint was prepared with the AAS LaTeX macros v3.0.

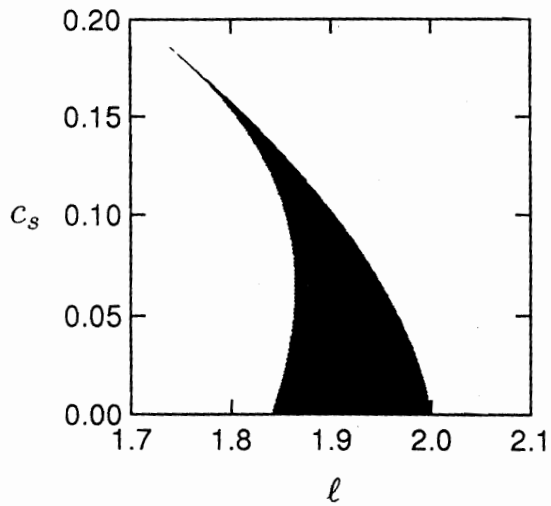

Fig. 2.— The number of steady state solutions is shown as a function of ℓ and c_s. There are triple steady state solutions for a given set of ℓ and c_s in the dark region while there is only one steady state solution in the blank region.

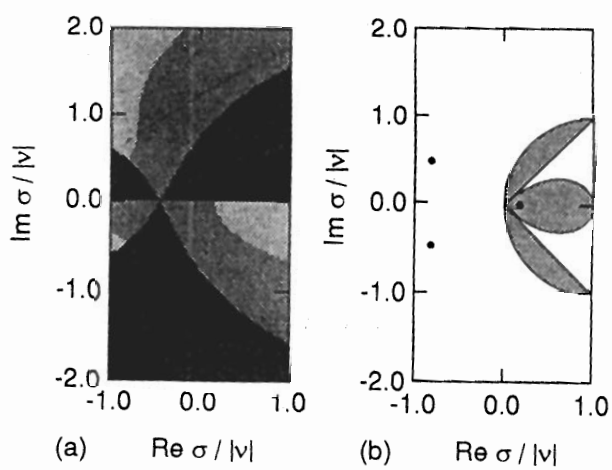

Fig. 3.— (a) The map of the eigenvalues on the complex σ plane for the inner shock wave solution of $c_s = 0.1\,c$ and $\ell = 1.87\,cr_g$. The abscissa and ordinate are the real and imaginary parts of σ in units of $\nu = -0.1848\,c/r_g$. The panel is painted with different greyness depending on the signatures of $\mathcal{R}_r$ and $\mathcal{R}_i$. The point of $\mathcal{R} = 0$ (the eigenvalue σ) appears as a quadruple point of four different greyness. (b) The eigenvalues are shown as filled circles on the complex σ plane. The grey regions denote the allowed regions for an unstable eigenmode (Nakayama 1992).

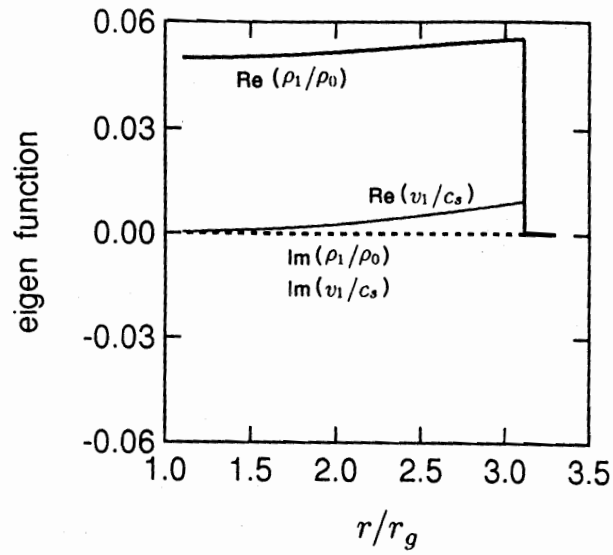

Fig. 4.— The eigenfunction of the unstable perturbation for the inner shock wave solution of $c_s = 0.1\,c$ and $\ell = 1.87\,cr_g$. The amplitude of the perturbation is normalized so that $\xi = -0.1\,r_g$. The abscissa and ordinate are the radial distance and the amplitude of the eigenfunction, ρ_1/ρ_0 and v_1/c_s. Both ρ_1/ρ_0 and v_1/c_s are real (not complex). The growth rate of this mode is $\sigma = 0.031\,c/r_g$.

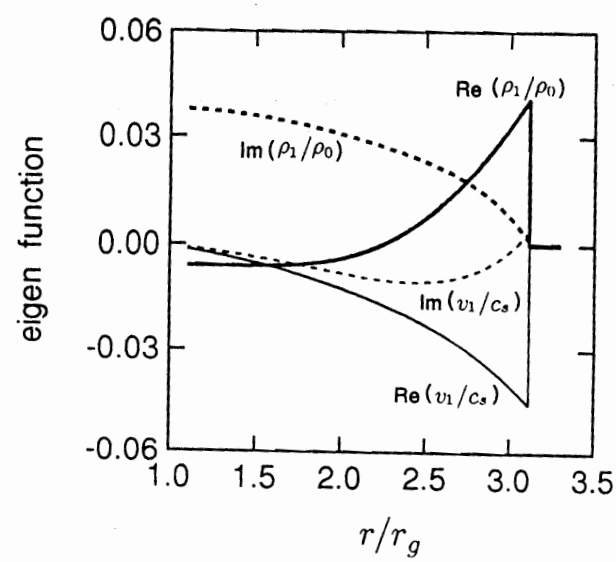

Fig. 5.— The same as figure 4 but for the damped oscillation whose eigenvalue is $\sigma = (-0.152 + 0.088i)\,c/r_g$. The amplitude is normalized so that $\xi = -0.1\,r_g$. The thick solid and dashed curves denote $\Re(\rho_1/\rho_0)$ and $\Im(\rho_1/\rho_0)$, respectively. The thin solid and dashed curves denote $\Re(v_1/c_s)$ and $\Im(v_1/c_s)$, respectively.

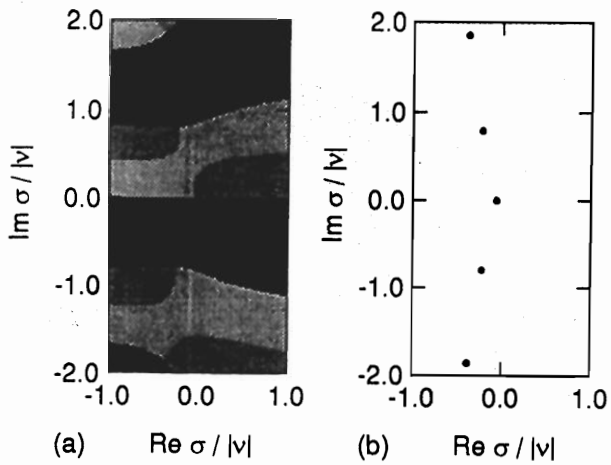

Fig. 6.— The same as figure 3 but for the outer shock wave solution of $c_s = 0.1\,c$ and $\ell = 1.87\,cr_g$. The units of the abscissa and ordinate are $\nu = 0.0588\,c/r_g$.

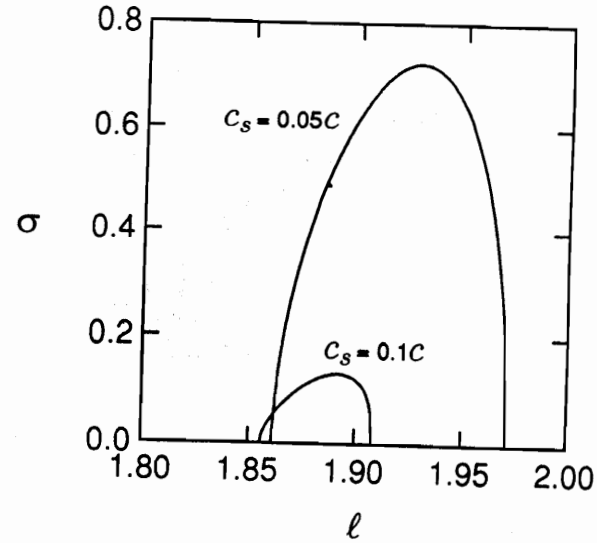

Fig. 7.— The growth rate of the unstable perturbation, σ as a function of ℓ. The growth rate is shown for $c_s = 0.1\,c$ and $0.05\,c$.

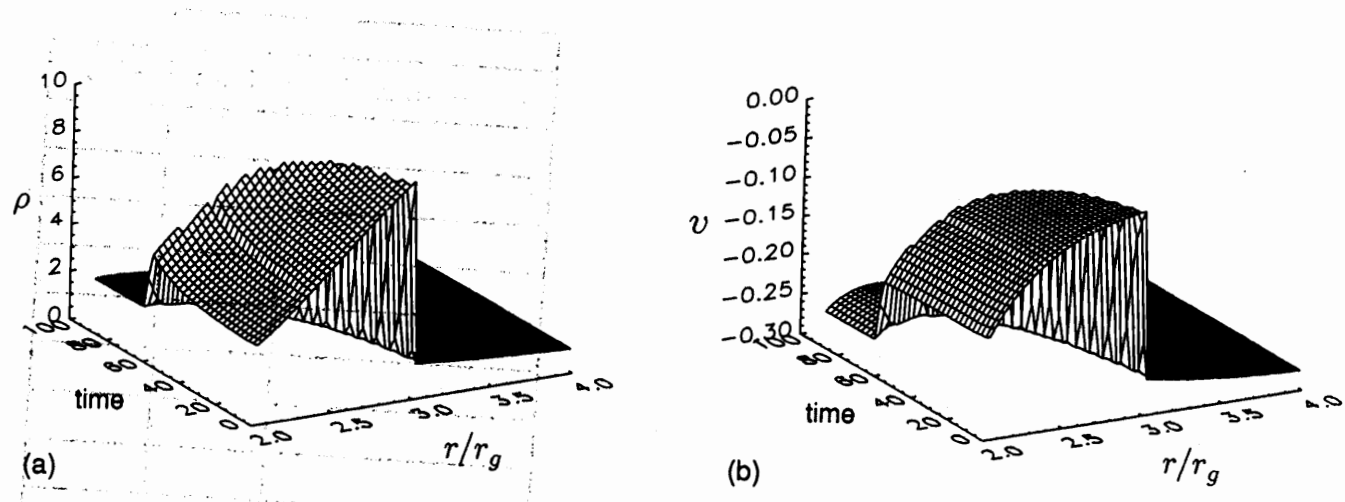

Fig. 8.— The nonlinear evolution of the unstable perturbation. The time evolution of the density (ρ) and velocity (v) are shown respectively in (a) and (b), respectively. Only a part of the numerical simulation is shown because of space. Grid spacing in the figure is $\Delta r = 0.03r_g$ and $\Delta t = 2.41r_g/c$ while the numerical simulation was performed with the resolution of $\Delta r = 0.03r_g$ and $\Delta t = 0.06r_g/c$. The shock front is shifted inward from the equilibrium position of the inner shock wave solution at the initial stage. The solution approaches to the no shock wave solution.

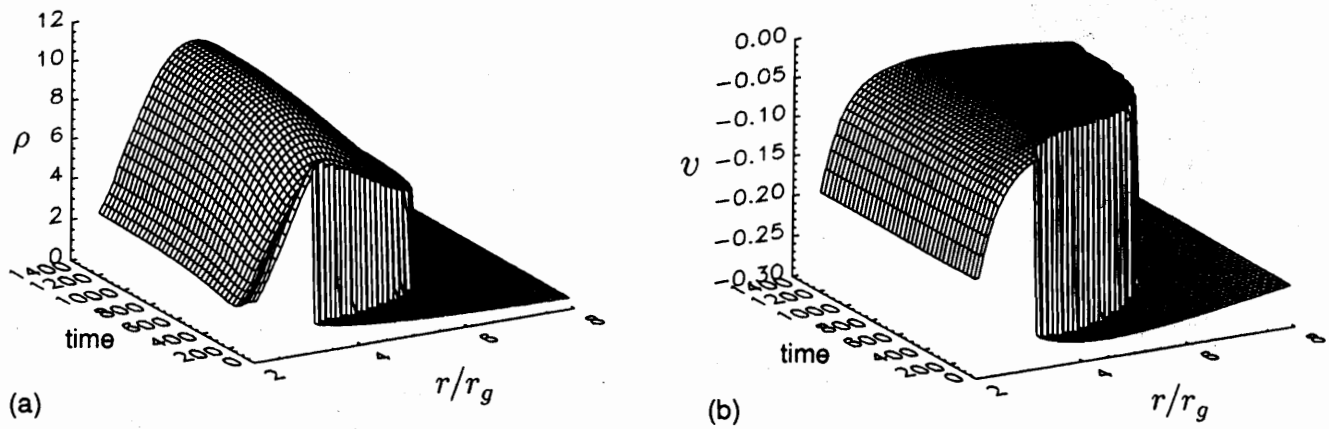

Fig. 9.— The same as figure 8 but for another example of the nonlinear simulation. Grid spacing in the figure is $\Delta r = 0.09 r_g$ and $\Delta t = 30.1 r_g/c$. The shock front is shifted outward from the equilibrium position of the inner shock wave solution. The solution approaches to the outer shock wave solution.

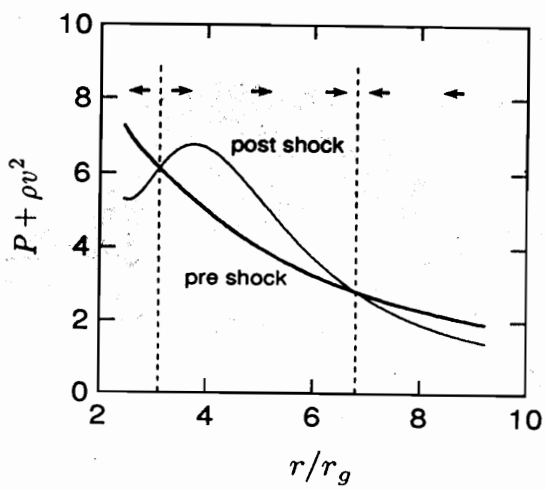

Fig. 10.— The total pressure distribution in the steady state for $c_s = 0.1\,c$ and $\ell = 1.87\,c r_g$. The ordinate is the sum of the thermal and ram pressure, $P + \rho v^2$. The abscissa is the radial coordinate. The thick and thin curves denote the pre- and post-shock flows, respectively. The arrows denote the expected motion of the shock front.

NAME | DATE | M.S.
RETURN TO FERMILAB LIBRARY